Nanoscale

Mechanically Strong and Electrically Conductive Multilayer MXene Nanocomposites

Journal:	*Nanoscale*
Manuscript ID	NR-ART-07-2019-006015.R1
Article Type:	Paper
Date Submitted by the Author:	09-Sep-2019
Complete List of Authors:	Lipton, Jason; New York University, Weng, Guo-Ming; New York University, Chemical and Biomolecular Engineering Alhabeb, Mohamed; A.J. Drexel Nanomaterials Institute, Drexel University, Materials Science and Engineering Maleski, Kathleen; A. J. Drexel Nanomaterials Institute, and Department of Materials Science and Engineering, Drexel University, Philadelphia, Pennsylvania 19104, United States, Antonio, Francisco; Yale University, Chemical and Environmental Engineering Kong, Jaemin; Yale University, Chemical and Environmental Engineering Gogotsi, Yury; A. J. Drexel Nanomaterials Institute, and Department of Materials Science and Engineering, Drexel University, Philadelphia, Pennsylvania 19104, United States, Taylor, Andre; New York University Tandon School of Engineering, Chemical and Biomolecular Engineering

ARTICLE

Mechanically Strong and Electrically Conductive Multilayer MXene Nanocomposites

Received 00th January 20xx,
Accepted 00th January 20xx

DOI: 10.1039/x0xx00000x

Jason Lipton[a,b], Guo-Ming Weng[a], Mohamed Alhabeb[c], Kathleen Maleski[c], Francisco Antonio[b], Jaemin Kong[a], Yury Gogotsi[c], and Andre D. Taylor[a]*

Polymer nanocomposites offer the opportunity to bridge properties of nanomaterials to the macroscale. In this work, layer-by-layer (LbL) assembly is used to demonstrate nanocomposites of 2D titanium carbide nanosheets (MXene) and clay nanoplatelets (montmorillonite) to fabricate freestanding thin films with unique multifunctional properties. These thin films can be tuned by adjusting the thickness to exhibit a tensile strength of 138 MPa - 225 MPa, EMI specific shielding effectiveness normalized to thickness and density up to 24,550 dB cm^2 g^{-1}, and sheet resistance from 855 Ω sq^{-1} – 3.27 kΩ sq^{-1} (corresponding to a range of conductivity from 53 S m^{-1} to 125 S m^{-1}). This composite is the strongest MXene-based LbL film prepared to date, in part due to the nacre-like brick-and-mortar structure. Ultra-strong, multifunctional films of this nature are desirable for many applications ranging from membranes, to structural and multifunctional composites, energy harvesting and storage, and materials for aerospace.

Introduction

The fabrication of polymer nanocomposites offers a unique opportunity to translate the advantageous properties of nanomaterials to the macroscale. Generally, the electrical and mechanical properties of polymer nanocomposites are inferior to the values of their nanoparticle components.[1] Layer-by-layer (LbL) assembly allows for control of the planar orientation and position of the nanoparticles in the composite, resulting in advantageous transfer of these properties from the particles to the bulk material.[2-4] LbL assembly is a scalable method for preparing polymer composites by sequentially coating a substrate in oppositely charged polyelectrolytes. When the polyelectrolyte solutions are designed to include dispersed nanoparticles, deposition of nanoparticle films of increasing thickness can be built after repeated coatings.[3,5,6]

In the past, LbL has been used to incorporate various nanomaterials such as clay nanoplatelets,[2,4] carbon nanotubes,[7] and graphene oxide[8] into polymer matrices to create strong composites. In particular, montmorillonite (MTM) clay nanoplatelets have been used in combination with poly(vinyl alcohol) (PVA) to create LbL composite materials with excellent strength, displaying tensile strengths as high as 400 MPa.[2] Recently, LbL composites of two-dimensional (2D) materials have drawn a great deal of interest due to the emergence of graphene.[9] However, aggregation of graphene sheets in solution prevents a large volume fraction from being evenly distributed in the polymer matrix, impairing the properties of the film.[2] Graphene oxide is commonly used as a solution-processable alternative to graphene, but reduction is required to establish electrical conductivity, necessitating the use of high temperatures or chemical reducing agents which may not be compatible with other components of the composite.[10] Further, metal nanoparticles have been used for LbL assembly in prior work for biosensing or surface enhanced Raman spectroscopy, but these films were not shown to be conductive or freestanding.[11,12] Thus, there have been limited reports of mechanically strong, freestanding, and conductive LbL films.

MXenes are a large family of 2D materials developed in 2011 with the chemical formula $M_{n+1}X_n$, where M is an early transition metal (Ti, V, Nb, Mo, Cr, etc.), X is carbon or nitrogen, and *n* is from 1 to 3.[13] Due to the wet chemical synthesis methods, MXenes exhibit surface functionalities such as oxygen, fluoride, or hydroxide groups, which impart hydrophilicity and allow for dispersion in water and polar organic solvents. Recently, it was shown non polar solvent dispersions of MXenes could be achieved *via* surface modification with silanes, introducing even more solution processing diversity.[14] As-produced Ti_3C_2 MXene has been shown to have freestanding film conductivities as high as 10,000 S cm^{-1}, a single flake Young's modulus greater than 330 GPa[15] (with theoretical values exceeding 500 GPa), and excellent performance as an electromagnetic interference (EMI) shielding material at µm thicknesses. These properties give MXenes a LbL solution processing advantage similar to graphene oxide, but with many orders of magnitude higher conductivity.[16–20] In addition, Ti_3C_2

[a] Department of Chemical and Biomolecular Engineering
New York University
Brooklyn, New York 11201, USA
[b] Department of Chemical and Environmental Engineering
Yale University
New Haven, Connecticut 06511, USA
[c] Department of Materials Science and Engineering and A.J. Drexel Nanomaterials Institute
Drexel University
Philadelphia, Pennsylvania 19104, USA
Electronic Supplementary Information (ESI) available:

MXene has been shown to be stable from oxidation when in solid film form,[21] enabling MXenes (and the corresponding composites) as attractive alternatives to common EMI shielding materials (e.g. Cu foil) which need large thicknesses to be effective.[22–25]

In this work, we demonstrate a multifunctional PVA-MTM-Ti_3C_2 MXene composite prepared by dip-LbL that has a very high tensile strength, tunable sheet resistance that is relatively low for an LbL film, and suitable performance as a lightweight EMI shielding material. In this composite, MTM imparts high tensile strength, PVA provides a flexible polymer binder, and MXenes also contribute to high strength, while enabling electrical conductivity and EMI shielding.[26] PVA was chosen because it has been demonstrated as a binder for high-strength conductive films when used in combination with Mxenes, CNTs, and other materials.[1,2,27] Multifunctional films of a desired number of bilayers were prepared by sequentially dipping a glass substrate into a pair of LbL solutions. The first solution contained PVA and Ti_3C_2, while the second solution contained MTM and Ti_3C_2. Ti_3C_2 was included in both dispersions to form a conductive network throughout the film. Photographs of the solutions are shown in Figure S1a. No phase separation is observed when they are left undisturbed for over 100 h (Figure S1b). Here, the PVA solution acts as the "positive" solution and the MTM as the "negative" solution,[2] resulting in growth of a film due to the electrostatic interactions between the adsorbed layer and materials in the bulk solution. The nomenclature of "positive" and "negative" solution is convenient for describing the mechanism of building for the LbL film, however the zeta potential data (Table S1) shows that both dispersions have a negative zeta potential. The MTM+Ti_3C_2 has a zeta potential of -49.1 mV and PVA + Ti_3C_2 has a zeta potential of -13.3 mV, thus the PVA solution is the "less-negative" solution. In reality, the driving force building the film is a complex mixture of hydrogen bonding, Van der Waals forces, and electrostatic interactions,[6,28] which we schematically illustrate as a brick-and-mortar structure (Figure 1a).

Experimental Methods

Solution preparation: 10 g of MTM powder was added to 1 L of deionized water (pH = 6.8) and stirred vigorously for at least one week until it was used for LbL.[2] Before LbL, 2 mg mL^{-1} Ti_3C_2 dispersion was mixed with the 1% MTM solution in a 1:1 volume ratio, resulting in a solution of 0.5% MTM, 1 mg mL^{-1} Ti_3C_2. 9 g of PVA was added into 400 mL of deionized water and heated at 80 °C while stirring until all particles were dissolved. This solution was mixed in a 1:1 volume ratio with 2 mg mL^{-1} Ti_3C_2 solution, resulting in a solution that has concentration of 1 mg mL^{-1} Ti_3C_2 and 1.25% PVA. The pH of the MTM/MXene and PVA/MXene solutions were measured to be 6.4 and 6.8, respectively.

Film Deposition: The glass slide substrates were first treated in piranha solution (3:1 H_2SO_4:H_2O_2) for 1 h, then thoroughly rinsed with deionized water. A typical deposition cycle would consist of dipping a clean substrate into the PVA solution for 5 min, drying under compressed air for 15 min, dipping in MTM solution for 5 min, and drying again under compressed air for 15 min. These steps result in the formation of 1 bilayer. This process was repeated until the desired number of bilayers were formed.

Preparation of freestanding films: After the desired number of bilayers had been deposited, the films were treated with 0.5% hydrofluoric acid (HF) solution for 2 h. This renders

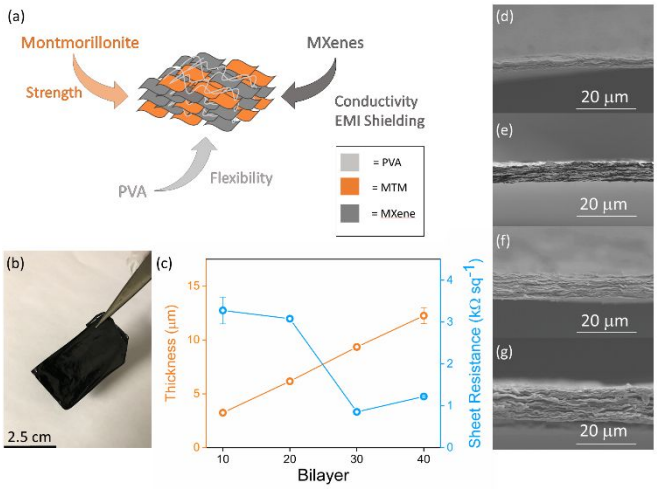

Figure 1. (a) Schematic brick-and-mortar internal structure of the nanocomposite film. (b) Digital photograph of freestanding nanocomposite. (c) Plot of bilayer number versus thickness (left y-axis) and sheet resistance (right y-axis). (d)-(g) cross-sectional SEM of 10, 20, 30, 40 bilayer freestanding films, respectively.

the surface of the substrate hydrophobic,[4] allowing for facile delamination of the film from the substrate. It is believed that such a gentle treatment could not cause any significant differences in the film structure and thus film properties (e.g. electric conductivity).[4] Additionally, we did not observe any dissolution of active materials during this HF treatment. After removal, the films were washed with DI water and dried under vacuum at room temperature for at least 24 h before mechanical testing. The density of the films prepared were 2.16 g cm^{-3}. All freestanding films shown in the results and discussion were prepared in the same way.

Results and Discussion

The films prepared using this technique show no visible evidence of phase separation (Figure 1b). There is a linear trend of increasing thickness with bilayer shown in Figure 1c, which is typical of the LbL deposition process. Using linear fitting, the thickness per bilayer was determined to be 272 nm. The large bilayer thickness can be attributed to the removal of the rinse step, which prevents dissolution of loosely-adsorbed species from the film between deposition steps. This is a strategy that has been employed in previous work to build freestanding LbL films.[7] The film thickness and nacre-like structure was characterized by SEM, shown in Figure 1d-g (enlarged SEM image shown in Figure S2). There is a trend of decreasing sheet resistance versus bilayer shown in Figure 1c, which levels off after 30 bilayers and reaches a low value of 855 Ω sq^{-1}. The sheet resistance plateau occurs because once there is an effective pathway for electrons to travel through the material, the addition of more conductive materials to improve this pathway has diminishing returns, similar to the percolation threshold effect seen in composites of carbon nanotubes.[29,30] The tunable thickness and sheet resistance

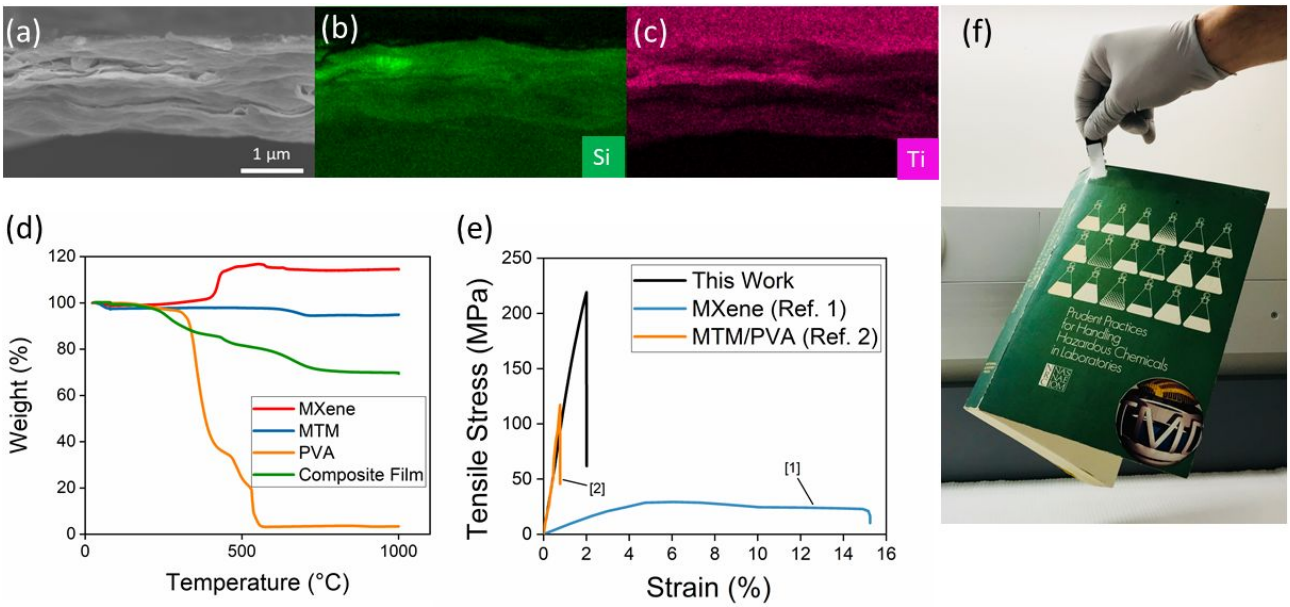

Figure 2. (a) Cross-sectional SEM image of a 10-bilayer film used for EDS. (b) EDS map of silicon and titanium (c) on the film cross-section. (d) TGA results of 50 bilayer PVA-MTM-Ti_3C_2 nanocomposite film and each individual component. (e) Stress-strain curve of a 10 bilayer PVA-MTM-Ti_3C_2 nanocomposite film. Stress-strain curves of a pure MXene film from ref. [1], and a LbL assembled PVA/MTM composite from ref. [2] are also shown for comparison. (f) Photograph of a 60-bilayer nanocomposite film supporting the weight of a 450 g book. The sample was attached to the book using label tape.

values correspond to a range of conductivity from 53 S m^{-1} to 125 S m^{-1}. This conductivity is lower than the theoretical value established for as-produced Ti_3C_2,[16] indicating that there is some intrinsic resistance in the layered structure arising from junction resistance between MXenes, and resistance of non-conductive fillers. It is important that both LbL solutions contain MXenes to allow bulk electronic conductivity, because the relatively thick bilayers cause the film to be insulating if Ti_3C_2 is not included in both layers.

Using energy dispersive x-ray spectroscopy (EDS), we confirm that the LbL solution components are incorporated into the final composite (Figure 2a-c). Si is representative of MTM, the chemical formula of which is $(Na,Ca)_{0.33}(Al,Mg)_2(Si_4O_{10})(OH)_2{\cdot}nH_2O$. The Ti is representative of Ti_3C_2. We note that the Si signal in the lower part of the Fig. 2b and Ti signal in the top part of Fig. 2c is a result of signal from exposed wrinkles of the film further away from the lens. Further, transmission electron microscopy (TEM) images with EDS elemental analysis of the individual MXene and MTM materials is shown in Figure S3. These images demonstrate the morphology and lateral size of the composite materials and verify that the elements chosen for EDS mapping in Figure 2b and 2c are appropriate.

Thermogravimetric analysis (TGA) measurements of the freestanding films in Figure 2d show that a large weight fraction of the composite is made up of the dispersed nanomaterials, i.e., 45.5% from MXenes and 17.6% from MTM [detailed calculations are shown in Equation (S1) - (S11) in the Supporting
Information]. Thus, the properties of the composite are largely a result of the properties of the nanomaterials themselves, as these materials together make up 63.1% of the mass of the film. LbL is an effective method to prepare composites having high nanomaterial loadings without aggregation, promoting optimal transfer of nanoscale properties to the bulk. It has been shown in prior LbL studies that adjusting the pH of the dipping solutions has the potential to adjust the individual layer thickness, so the mass ratios in this composite could

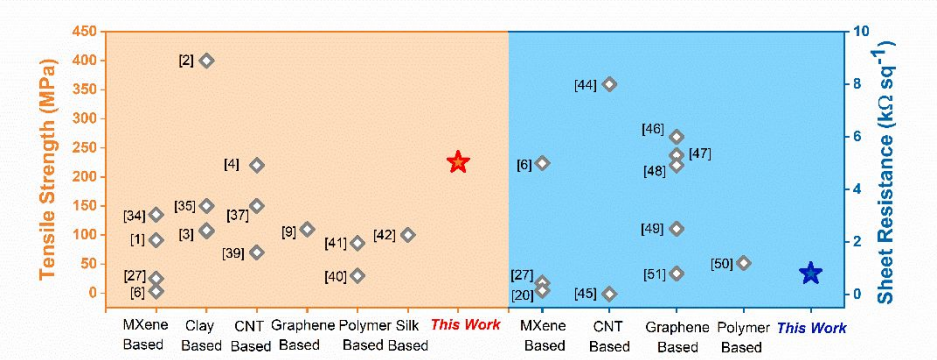

Figure 3. Comparison of (a) ultimate tensile strength, and (b) sheet resistance properties of LbL films in the literature. Note that two examples of MXene composite films are not prepared by LbL but have been included due to a lack of published data about LbL MXene composites. Numerical values are shown in Table S2.

similarly be adjusted in such a manner.[31] Using solution pH to tune the MXene quantity in LbL nanocomposite films presents an opportunity for further study of the demonstrated materials system, as well as other similar systems. We note that there is an increase in MXene mass of 15% during TGA measurement in air due to oxidation of titanium. This has been observed previously for TGA data of MXenes.[32]

The mechanical properties of the freestanding nanocomposites were analyzed using uniaxial tensile testing. We show the stress-strain curve (Figure 2e), and the image of the film holding up a 450 g book (Figure 2f and Video S1) which demonstrates that the high ultimate tensile strength of this nanocomposite material is unrivaled by any previously prepared MXene film (as discussed below). From the relatively high strength of the MTM-PVA film compared to the MXene film referenced in Figure 2e, it is clear MTM plays a significant role in enhancing the strength of the PVA-MTM-Ti_3C_2 composite. The 10-bilayer (~3 µm) composite has an average ultimate tensile strength of 225 ± 25 MPa, and Young's modulus 10.5 ± 6.6 GPa. There is a trend of decreasing strength from 225 MPa to 138 MPa with increasing bilayer number from 10 to 40, which is consistent with other studies on thin films (Figure S4).[33] This composite film breaks at low strain, indicating utility in an application requiring a stiff film that does not deform before breakage. The composite from this work, containing all three of the components, shows a higher ultimate tensile strength than a LbL PVA/MTM composite and as-produced MXene freestanding film from previous reports (Figure 2e).[1,2] We note that an MTM/MXene control film cannot be prepared through LbL due to the large negative zeta potential of both components (Table S1).[4,34,35] Additionally, a PVA/MTM/MXene control film cannot be reproducibly prepared through vacuum assisted filtration (the most common method of MXene freestanding film preparation)[36] because the majority of the solubilized polymer will go through the 0.22 µm pore-size filter membrane, thus the MXene composite is uniquely suited to be prepared through LbL assembly. This MXene composite film could be deriving its strength from similar structural properties to nacre, in that there are interactions of MXenes and MTM with the polymer matrix, and structural similarities between the materials. Non-bonding interactions of MXenes and MTM with the polymer matrix allows for stress transfer from the polymer to the high-strength nanomaterials, along with interaction between the platelets themselves in a manner similar to nacre.[37] The length scales are also similar to those in nacre. According to dynamic light scattering (DLS) the MTM particles are 410 nm in diameter on average, the MXene flakes are 1.1 µm in diameter on average (Figure S5), and the aragonite bricks of nacre are 2.5 µm.[37]

We illustrate that this combination of high strength and low sheet resistance is in the top-tier for an LbL film, as can be seen in the literature comparison of Figure 3. To offer a comparison of this multifunctional material with others in the literature, we make a comparison of different classification criteria (Figure 3), in which we separate the data into two panels, one for each property. This material is the among the

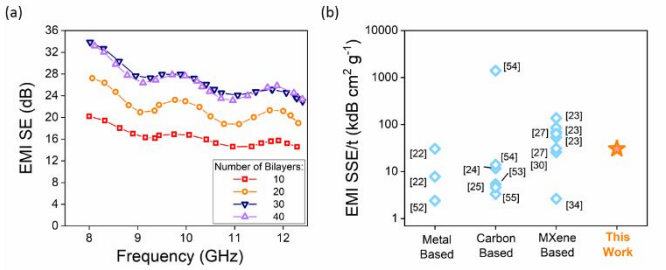

Figure 4. (a) EMI SE of 10-40 bilayer nanocomposite films. (b) Comparison of EMI SSE/t of this film to other materials in the literature.

leaders of strong LbL films (thickness information and data in numerical form shown in Table S2). We note that we can readily adjust the sheet resistance towards the lowest values achieved by LbL films by dding additional bilayers (Figure 3b). It is clear that combination of MTM, PVA, and Mxene results in a high tensile strength film, but the addition of non-conductive fillers inhibits the conductivity. In addition to high strength and conductivity, we examined this MXene composite for its performance as an EMI shielding material.

We examine the shielding effectiveness of the composite in the frequency range of 8-12.4 GHz using the testing setup outlined in the supplementary information and shown in Figure S6. This is an important frequency range for military and commercial applications.[27] The shielding efficiency increases with the bilayer number until 30 bilayers, and then not much change is seen between 30 and 40 bilayers (Figure 4a). There is a correlation between conductivity and EMI SE[22] [shown in Equation (S12) of the supporting information), therefore, it is reasonable for the shielding efficiency to level off after 30 bilayers, consistent with the trend of sheet resistance versus bilayer number. Additionally, as can be seen in Figure 4b, the specific EMI SE normalized to the thickness and density (EMI SSE/t) outperforms carbon based and metal foil materials and is competitive with some recent MXene materials. A 20 bilayer film exceeds 20 dB of attenuation (accepted in the EMI shielding community to be the standard of useful shielding).[38] We propose that the EMI shielding happens due to the absorption of electromagnetic waves into the layered polymer nanocomposite with embedded MXenes.[22] This is a reasonable conclusion since the MTM and PVA are not electrically conductive, and therefore could not contribute to EMI shielding.[22,39]

Conclusion

In summary, we demonstrate a high-strength, freestanding, conductive, polymer nanocomposite material prepared by a LbL assembly method using MTM clay nanoplatelets, Ti_3C_2 nanosheets, and PVA. The freestanding films can be tuned to have ultimate tensile strength of 225 ± 25 MPa, or a sheet resistance of 855 Ω sq^{-1}, and average EMI shielding effectiveness of 26.9 dB. This is the strongest LbL composite film prepared to date using MXenes. The high strength, along with the good electrical and EMI shielding properties make it a promising material to use in a variety of

applications requiring a multifunctional material. We envision further optimization can be carried out to optimize this system towards a specific application and provide these demonstrations as some possible considerations for this new materials system.

Conflicts of Interest

There are no conflicts to declare.

Acknowledgements

The authors would like to acknowledge Dr. M. Lee and the Yale Materials Characterization Corps for their assistance. The authors would like to acknowledge Dr. S.Y. Kim, G. Weston-Murphy, and K. Ryan for their assistance with tensile testing, and Dr. C. Axline and Prof. R. Schoelkopf for his help with EMI shielding measurements. Additionally, the authors would like to acknowledge BYK USA inc., for supplying the samples of Na^+- closite (MTM) and Simge Uzun (Drexel) for help with MXene sample preparation.

References

1 1 Z. Ling, C. E. Ren, M. Zhao, J. Yang, J. M. Giammarco, J. Qiu, M. W. Barsoum and Y. Gogotsi, *Proc. Natl. Acad. Sci.*, 2014, **111**, 16676–16681.

2 P. Podsiadlo, A. K. Kaushik, E. M. Arruda, A. M. Waas, B. S. Shim, J. Xu, H. Nandivada, B. G. Pumplin, J. Lahann, A. Ramamoorthy and N. A. Kotov, *Science*, 2007, **318**, 80–83.

3 A. A. Mamedov, N. A. Kotov, M. Prato, D. M. Guldi, J. P. Wicksted and A. Hirsch, *Nat. Mater.*, 2002, **1**, 190–194.

4 Z. Tang, N. A. Kotov, S. Magonov and B. Ozturk, *Nat. Mater.*, 2003, **2**, 413–418.

5 J. J. Richardson, M. Björnmalm and F. Caruso, *Science*, 2015, **348**, 1–11.

6 Z. Zhou, W. Panatdasirisuk, T. S. Mathis, B. Anasori, C. Lu, X. Zhang, Z. Liao, Y. Gogotsi and S. Yang, *Nanoscale*, 2018, 6005–6013.

7 A. D. Taylor, M. Michel, R. C. Sekol, J. M. Kizuka, N. A. Kotov and L. T. Thompson, *Adv. Funct. Mater.*, 2008, **18**, 3003–3009.

8 T. Guin, B. Stevens, M. Krecker, J. D'Angelo, M. Humood, Y. Song, R. Smith, A. Polycarpou and J. C. Grunlan, *ACS Appl. Mater. Interfaces*, 2016, **8**, 6229–6235.

9 Y. Xu, W. Hong, H. Bai, C. Li and G. Shi, *Carbon*, 2009, **47**, 3538–3543.

10 H. A. Becerril, J. Mao, Z. Liu, R. M. Stoltenberg, Z. Bao and Y. Chen, *ACS Nano*, 2008, **2**, 463–70.

11 P. H. B. Aoki, P. Alessio, J. A. de Saja and C. J. L. Constantino, *J. Raman Spectrosc.*, 2010, **41**, 40–48.

12 J. Zhao, X. Kong, W. Shi, M. Shao, J. Han, M. Wei, D. G. Evans and X. Duan, *J. Mater. Chem.*, 2011, **21**, 13926–13933.

13 M. Naguib, M. Kurtoglu, V. Presser, J. Lu, J. Niu, M. Heon, L. Hultman, Y. Gogotsi and M. W. Barsoum, *Adv. Mater.*, 2011, **23**, 4248–4253.

14 S. Lim, H. Park, J. Yang, C. Kwak and J. Lee, *Colloids Surfaces A Physicochem. Eng. Asp.*, 2019, 123648.

15 A. Lipatov, H. Lu, M. Alhabeb, B. Anasori, A. Gruverman, Y. Gogotsi and A. Sinitskii, *Sci. Adv.*, 2018, **4**, 1–7.

16 B. Anasori, M. R. Lukatskaya and Y. Gogotsi, *Nat. Rev. Mater.*, 2017, **2**, 1–17.

17 K. Chaudhuri, M. Alhabeb, Z. Wang, V. M. Shalaev, Y. Gogotsi and A. Boltasseva, *ACS Photonics*, 2018, **5**, 1115–1122.

18 K. Maleski, V. N. Mochalin and Y. Gogotsi, *Chem. Mater.*, 2017, **29**, 1632–1640.

19 M. Mariano, O. Mashtalir, F. Antonio, W.-H. Ryu, B. Deng, F. Xia, Y. Gogotsi and A. Taylor, *Nanoscale*, 2016, **8**, 16371–16378.

20 W. Tian, A. VahidMohammadi, Z. Wang, L. Ouyang, M. Beidaghi and M. M. Hamedi, *Nat. Commun.*, 2019, **10**, 2558.

21 C. J. Zhang, S. Pinilla, N. McEvoy, C. P. Cullen, B. Anasori, E. Long, S. H. Park, A. Seral-Ascaso, A. Shmeliov, D. Krishnan, C. Morant, X. Liu, G. S. Duesberg, Y. Gogotsi and V. Nicolosi, *Chem. Mater.*, 2017, **29**, 4848–4856.

22 F. Shahzad, M. Alhabeb, C. B. Hatter, B. Anasori, S. Man Hong, C. M. Koo and Y. Gogotsi, *Science*, 2016, **353**, 1137–1140.

23 Y.-T. Liu, P. Zhang, N. Sun, B. Anasori, Q. Zhu, H. Liu, Y. Gogotsi and B. Xu, *Adv. Mater.*, 2018, **30**, 1707334.

24 Y. Li, X. Pei, B. Shen, W. Zhai, L. Zhang and W. Zheng, *RSC Adv.*, 2015, **5**, 24342–24351.

25 M. Crespo, M. González, A. L. Elías, L. Pulickal Rajukumar, J. Baselga, M. Terrones and J. Pozuelo, *Phys. Status Solidi - Rapid Res. Lett.*, 2014, **8**, 698–704.

26 W. Tian, A. VahidMohammadi, M. S. Reid, Z. Wang, L. Ouyang, J. Erlandsson, T. Pettersson, L. Wågberg, M. Beidaghi and M. M. Hamedi, *Adv. Mater.*, 2019, **1902977**, 1902977.

27 G.-M. Weng, J. Li, M. Alhabeb, C. Karpovich, H. Wang, J. Lipton, K. Maleski, J. Kong, E. Shaulsky, M. Elimelech, Y. Gogotsi and A. D. Taylor, *Adv. Funct. Mater.*, 2018, **28**, 1803360.

28 N. Miyake, T. Miura, T. Sato and M. Yoshinari, *J. Biomed. Sci. Eng.*, 2013, **6**, 273–276.

29 F. S. Gittleson, D. J. Kohn, X. Li and A. D. Taylor, *ACS Nano*, 2012, **6**, 3703–3711.

30 M. Zurita-Gotor, F. S. Gittleson, A. D. Taylor and J. Blawzdziewicz, *Phys. Rev. B - Condens. Matter Mater. Phys.*, 2013, **87**, 1–9.

31 S. S. Shiratori and M. F. Rubner, *Macromolecules*, 2000, **33**, 4213–4219.

32 M. Naguib, T. Saito, S. Lai, M. S. Rager, T. Aytug, M. Parans Paranthaman, M.-Q. Zhao and Y. Gogotsi, *RSC Adv.*, 2016, **6**, 72069–72073.

33 Y. Choi and S. Suresh, *Acta Mater.*, 2002, **50**, 1881–1893.

34 W. Cao, F.-F. Chen, Y. Zhu, Y.-G. Zhang, Y. Jiang, M.-G. Ma and F. Chen, *ACS Nano*, 2018, **12**, 4583–4593.

35 A. Walther, I. Bjurhager, J. M. Malho, J. Ruokolainen, L. Berglund and O. Ikkala, *Angew. Chemie - Int. Ed.*, 2010, **49**, 6448–6453.

36 M. Alhabeb, K. Maleski, B. Anasori, P. Lelyukh, L. Clark, S.

Sin and Y. Gogotsi, *Chem. Mater.*, 2017, **29**, 7633–7644.
37 K. S. Katti and D. R. Katti, *Mater. Sci. Eng. C*, 2006, **26**, 1317–1324.
38 J. Liang, Y. Wang, Y. Huang, Y. Ma, Z. Liu, J. Cai, C. Zhang, H. Gao and Y. Chen, *Carbon N. Y.*, 2009, **47**, 922–925.
39 J. Yeh, C. Chin and S. Chang, *J. Appl. Polym. Sci.*, 2016, **88**, 3264–3272.
36 T. U. Patro and H. D. Wagner, *Nanotechnology*, 2011, **22**, 1–12.
37 M. Olek, J. Ostrander, S. Jurga, H. Möhwald, N. Kotov, K. Kempa and M. Giersig, *Nano Lett.*, 2004, **4**, 1889–1895.
38 B. S. Shim, Z. Tang, M. P. Morabito, A. Agarwal, H. Hong and N. A. Kotov, *Chem. Mater.*, 2007, **19**, 5467–5474.
39 M. K. Gheith, V. A. Sinani, J. P. Wicksted, R. L. Matts and N. A. Kotov, *Adv. Mater.*, 2005, **17**, 2663–2670.
40 H. Y. Park, Jong Hoon; Kim, Byoung Suhk; Yoo, Yeon Chun; Khil, Myung Seob; Kim, *J. Appl. Polym. Sci.*, 2008, **107**, 2211–2216.
41 P. Podsiadlo, E. M. Arruda, E. Kheng, A. M. Waas, Ǵ. J. Lee, K. Critchley, M. Qin, E. Chuang, A. K. Kaushik, H. Kim, Œy. Qi, S. Noh and N. A. Kotov, *ACS Nano*, 2009, **3**, 1564–1572.
42 C. Jiang, X. Wang, R. Gunawidjaja, Y. H. Lin, M. K. Gupta, D. L. Kaplan, R. R. Naik and V. V Tsukruk, *Adv. Funct. Mater.*, 2007, **17**, 2229–2237.
43 H. An, T. Habib, S. Shah, H. Gao, M. Radovic, M. J. Green and J. L. Lutkenhaus, *Sci. Adv.*, 2018, **4**, 1–9.
44 T. Hong, D. W. Lee, H. J. Choi, H. S. Shin and B. Kim, ACS Nano, 2010, **4**, 3861–3868.
45 C. Cho, B. Stevens, J. H. Hsu, R. Bureau, D. A. Hagen, O. Regev, C. Yu and J. C. Grunlan, *Adv. Mater.*, 2015, **27**, 2996–3001.
46 K. Sheng, H. Bai, Y. Sun, C. Li and G. Shi, *Polymer.*, 2011, **52**, 5567–5572.
47 A. K. Sarker and J. D. Hong, *Langmuir*, 2012, **28**, 12637–12646.
48 B. Stevens, E. Dessiatova, D. A. Hagen, A. D. Todd, C. W. Bielawski and J. C. Grunlan, *ACS Appl. Mater. Interfaces*, 2014, **6**, 9942–9945.
49 D. W. Lee, T.-K. Hong, D. Kang, J. Lee, M. Heo, J. Y. Kim, B.-S. Kim and H. S. Shin, *J. Mater. Chem.*, 2011, **21**, 3438–3442.
50 J.-Y. Hong, K.-Y. Shin, O. S. Kwon, H. Kang and J. Jang, *Chem. Commun.*, 2011, **47**, 7182–7184.
51 Y. Zhou, J. Yang, X. Cheng, N. Zhao, H. Sun and D. Li, *RSC Adv.*, 2013, **3**, 3391–3398.
52 J. Ma, K. Wang and M. Zhan, *RSC Adv.*, 2015, **5**, 65283–65296.
53 Z. Zeng, H. Jin, M. Chen, W. Li, L. Zhou and Z. Zhang, *Adv. Funct. Mater.*, 2016, **26**, 303–310.
54 B. Shen, Y. Li, D. Yi, W. Zhai, X. Wei and W. Zheng, *Carbon*, 2016, **102**, 154–160.
55 Z. Chen, C. Xu, C. Ma, W. Ren and H. M. Cheng, *Adv. Mater.*, 2013, **25**, 1296–1300.

A high-strength composite is formed by the hierarchical assembly of electrically conductive two-dimensional MXenes in a nacre-inspired structure.